Magnetic properties of the weak itinerant-electron ferromagnet $Ni_{75}Al_{25}$: I. The effect of site disorder

2004 J. Phys.: Condens. Matter 16 8675

(http://iopscience.iop.org/0953-8984/16/47/019)

INSTITUTE OF PHYSICS PUBLISHING JOURNAL OF PHYSICS: CONDENSED MATTER

J. Phys.: Condens. Matter **16** (2004) 8675–8694 PII: S0953-8984(04)75112-7

Magnetic properties of the weak itinerant-electron ferromagnet $Ni_{75}Al_{25}$: I. The effect of site disorder

Anita Semwal and S N Kaul[1]

School of Physics, University of Hyderabad, Central University PO, Hyderabad-500 046, Andhra Pradesh, India

E-mail: kaulsp@uohyd.ernet.in

Received 19 January 2004, in final form 21 May 2004
Published 12 November 2004
Online at stacks.iop.org/JPhysCM/16/8675
doi:10.1088/0953-8984/16/47/019

Abstract

Extensive magnetization measurements have been performed over wide ranges of temperature and magnetic field on polycrystalline $Ni_{75}Al_{25}$ samples 'prepared' in different states of site disorder and thoroughly characterized by x-ray diffraction (XRD), x-ray fluorescence and inductively coupled plasma optical emission spectroscopy. Detailed analysis of the magnetization (XRD) data permits an accurate determination of the spontaneous magnetization, M_0, zero-field differential susceptibility, χ_0, and spin wave stiffness, D_0, at 0 K, Curie temperature, T_C, density of states (DOS) at the Fermi level, $N(E_F)$ (the atomic long-range order parameter, **S**, which is a direct measure of the site disorder present). The effect of site disorder on the ground-state as well as the finite-temperature magnetic properties of $Ni_{75}Al_{25}$ is clearly brought out by the observed variations of M_0, χ_0, D_0, T_C and $N(E_F)$ with **S**. The main findings are as follows. Site disorder smears out the sharp features in the DOS curve near the Fermi level, E_F, reduces $N(E_F)$ and thereby promotes both propagating transverse spin fluctuations (spin waves) and non-propagating zero-point as well as thermally excited spin fluctuations. The reduction in $N(E_F)$, in turn, results in diminished (enhanced) values of M_0, D_0 and $T_C(\chi_0)$ with increased site disorder. Site disorder only affects the magnitude of the suppression of spin waves and thermally excited spin fluctuations by the magnetic field (H) but does not alter the functional form of the suppression with field. This functional dependence on field is $\sqrt{H}$ for spin waves at low temperatures and slows down from a linear variation ($\sim H$) at intermediate temperatures to a $\sqrt{H}$ variation at temperatures close to T_C for the thermally excited spin fluctuations. Another important observation is that all the physical quantities of interest such as M_0, χ_0, D_0, T_C and $N(E_F)$ exhibit a sizable change in their magnitudes when point defects such as vacancies play an important role in enhancing the degree of site disorder.

[1] Author to whom any correspondence should be addressed.

1. Introduction

The most extensively studied intermetallic compound among the compounds MnSi, Ni_3Al, NiPt, Sc_3In and $ZrZn_2$ that exhibit weak itinerant-electron (WI) ferromagnetism is Ni_3Al. γ'-Ni_3Al crystallizes in a $L1_2$ Cu_3Au-type face-centred-cubic (fcc) structure. In a completely *ordered* Ni_3Al compound, Ni and Al atoms occupy the face centres and corners of the fcc unit cell. The corner sites and face-centre sites thus form two separate but interpenetrating Al and Ni sublattices. An important property of this compound is that it undergoes a structural *order–disorder* phase transition at a temperature $T_{od} \approx 1450\,^{\circ}C$. In the disordered phase, the probability of Ni (Al) atoms occupying the face-centre (corner) sites is *less* than unity. A *completely disordered* state corresponds to the case when Ni and Al atoms occupy the fcc lattice sites with *equal* probability. Consequently, the samples of $Ni_{75}Al_{25}$ prepared by the techniques in which the molten alloy is quenched at widely different rates are bound to be in different states of site disorder. Now that the Ni atoms alone carry magnetic moment in this compound, atomic site disorder gives rise to quenched random-exchange disorder, which, in turn, is expected to have a profound effect on the ground-state as well as the finite-temperature magnetic properties of $Ni_{75}Al_{25}$. That this is indeed the case is borne out by the following experimental observations.

Early magnetic investigations [1, 2] on plastically deformed $Ni_{75}Al_{25}$ revealed that the long-range ferromagnetic order is completely destroyed and a superparamagnetic behaviour persists at temperatures down to 4.2 K. Recently, a detailed comparative bulk magnetization study [3] of (*disordered*) nanocrystalline and (*ordered*) polycrystalline samples of Ni_3Al demonstrated that the long-range ferromagnetic order, prevalent in the polycrystalline samples, breaks down completely in the nanocrystalline counterpart, which instead exhibits exchange-enhanced Pauli spin paramagnetism for $T \geqslant 5$ K. In view of the above remarks, a meaningful comparison between the experimental results reported for the samples of Ni_3Al prepared by different techniques and hence possessing varied amounts of site disorder is possible only when the effect of quenched random-exchange disorder on the physical properties of the system in question is known *a priori*.

On the theoretical front, a recent self-consistent calculation [4] of the zero-point (ZP) and thermally excited (TE) spin fluctuations in WI ferromagnets in the presence and absence of an external magnetic field goes far beyond the 'conventional' spin fluctuation theories [5, 6] in that it makes specific predictions about the roles of ZP and TE spin fluctuations in the thermal demagnetization of WI ferromagnets and about the sensitivity of these components of spin fluctuations to the magnetic field. These theoretical predictions were later confirmed by the results of a detailed experimental investigation [7] of the nature of low-lying magnetic excitations in the polycrystalline samples of *ordered* Ni_3Al. Though this comparison between theory and experiment has resolved many outstanding issues concerning weak itinerant-electron ferromagnetism in Ni_3Al by bringing out clearly certain attributes *inherent* to this WI ferromagnet, none of the theoretical attempts made so far has addressed the basic issue of the influence of site disorder (or equivalently, quenched random-exchange disorder) on the magnetic properties of WI ferromagnets.

The above considerations prompted us to undertake an extensive bulk magnetization study of the polycrystalline samples of $Ni_{75}Al_{25}$, which differ in the degree of site disorder. An elaborate analysis of the magnetization and ac susceptibility data taken in the critical region and at temperatures well above the Curie temperature, T_C, for these samples reveals [8] that the site disorder alters neither the critical behaviour of the ordered Ni_3Al nor the degree of itinerancy of the magnetic electrons (as inferred from the paramagnetic-to-ferromagnetic magnetic moment ratio). The present paper basically aims at unravelling the effect of quenched

random-exchange disorder on the ground-state and finite-temperature ($T < T_C$) magnetic properties of $Ni_{75}Al_{25}$.

2. Experimental details

One set of spheres and discs of the so-called 'as-prepared' polycrystalline $Ni_{75}Al_{25}$ sample, whose preparation details are given elsewhere [8], was subjected to annealing treatment at 520 °C for 16 days in quartz tubes evacuated to a pressure of 10^{-6} Torr, in order to achieve the *maximum* degree of atomic order in the sample. A portion of the 'as-prepared' polycrystalline $Ni_{75}Al_{25}$ rod was melted by a radio-frequency induction-melting technique in a quartz tube under an inert (99.999% pure helium gas) atmosphere maintained at a base pressure of 100 mbar. The molten alloy was ejected at a temperature of 1500 °C and a helium pressure of 200 mbar from a slit of dimensions 3.1×0.47 mm^2 in the quartz tube onto a copper wheel of diameter 20 cm, rotating at a speed of 18 000 rpm (amounting to a tangential velocity of 30 m s^{-1}) and maintained at 20 °C with a water cooling arrangement. Long high-quality ribbons of 1.5 mm width and 28 μm thickness were thus prepared in a *disordered state* by rapid quenching of the melt. The samples in the 'as-prepared', 'annealed' and 'quenched' states are henceforth referred to as S_0, S_1 and S_2, respectively.

In order to ascertain whether the actual composition of the samples conforms to the nominal composition $Ni_{75}Al_{25}$, a detailed compositional analysis was carried out using the x-ray fluorescence technique and inductively coupled plasma optical emission spectroscopy. This analysis revealed that

(i) all three samples had the *same* composition $Ni_{75.08}Al_{24.92}$ within the experimental resolution limit of ± 0.09 (± 0.05) for Ni (Al) and
(ii) the total concentration of magnetic 3d transition metal impurities such as Mn, Cr, Fe and Co did not exceed 0.002 at.%.

While result (i) is not surprising considering the fact that all three samples come from the *same* source ('as-prepared' polycrystalline $Ni_{75}Al_{25}$ rod), low impurity concentration is consistent with the 99.998% purity of the starting materials Ni and Al. X-ray diffraction (XRD) patterns recorded for these samples at room temperature using Cu Kα radiation have already been reported [8] earlier.

The magnetization, M, of the polycrystalline samples S_1 (spherical in shape with a diameter of 3 mm) and S_2 (in the form of ribbon pieces, each of dimensions $2.2 \times 1.8 \times 0.028$ mm^3, stacked one above the other and glued together with Apeizon N grease) was measured as a function of the external magnetic field, H_{ext}, in fields up to 15 kOe at *fixed* temperatures spaced 0.5, 0.1 and 0.05 K apart in the ranges 14 K $\leqslant T \leqslant 0.5T_C$, $0.5T_C \leqslant T \leqslant 0.8T_C$ and $0.8T_C \leqslant T \leqslant T_C$, respectively, on a vibrating sample magnetometer (VSM). M–H_{ext} isotherms were taken for all three samples S_0 (sphere of 3 mm diameter), S_1 and S_2 at $T = 5$ K in fields up to 70 kOe using a SQUID magnetometer. Magnetization was also measured as a function of temperature in temperature steps of 0.25 and 0.5 K in the intervals 14 K $\leqslant T \leqslant T_C - 5$ K and $T_C - 5$ K $\leqslant T \leqslant T_C + 20$ K, respectively, at *fixed* values of H_{ext}, 0.5 kOe apart, in the range 0.5 kOe $\leqslant H_{ext} \leqslant 4$ kOe with a VSM for the samples S_1 and S_2 and in 0.25 K steps in the temperature range 5 K $\leqslant T \leqslant 100$ K at $H_{ext} = 1$ kOe with a SQUID magnetometer for all the samples. The 'in-field' magnetization data, so obtained, are denoted by $M(T, H_{ext})$. In the above measurements, the temperature and magnetic field stabilities were better than ± 5 mK (± 10 mK) and ± 1 Oe (± 1 Oe), respectively, for the VSM (SQUID) data. The M–H_{ext} isotherms for the samples S_1 and S_2 were converted into magnetization versus temperature data at 60 different but *fixed* values of H_{ext} in the interval

Table 1. The atomic long-range order parameter, **S**, lattice parameter, a, magnetic moment per Ni atom at 5 K, μ_{Ni}, coefficient of the $\sqrt{H}$ term in equation (1), η', and high-field susceptibility, χ_{hf}, (equation (1)).

Sample	**S**	a (Å)	μ_{Ni} (μ_B)	η' (10^{-2} Oe$^{-1/2}$)	χ_{hf} (10^{-5})
S_0	0.84(4)	3.5665(10)	0.0882(3)	3.4(3)	8.0(3)
S_1	0.95(2)	3.5650(15)	0.0775(2)	4.1(1)	7.0(3)
S_2	0.76(4)	3.5650(10)	0.0521(4)	7.0(5)	5.2(2)

0.03 kOe $\leqslant H_{ext} \leqslant$ 15 kOe. Such data are henceforth referred to as the 'in-field (iso)' magnetization data and labelled as $M'(T, H_{ext})$. The demagnetizing factor N of the samples was computed from the *inverse slope* of the M–H_{ext} straight line isotherm taken at the lowest temperature (14 K) in the field range -20 Oe $\leqslant H_{ext} \leqslant 20$ Oe. The values of N so obtained were used to calculate the effective field, H, from the relation $H = H_{ext} - 4\pi NM(T, H_{ext})$.

3. Data analysis, results and discussion

The observed XRD patterns could be completely indexed [8] on the basis of the $L1_2$ cubic structure. Refined values of the lattice parameter a for all the samples, obtained [8] by employing the well-known Nelson–Riley–Taylor–Sinclair method [9], are displayed in table 1. The values of long-range order parameter, **S** (which is a direct measure of the degree of order, and hence of disorder, present), listed in table 1 have been deduced from the observed *integrated* intensities of the superstructure and fundamental Bragg reflection peaks by an elaborate procedure whose details are given in [8] and [10]. According to the general definition $\mathbf{S} = (r - w)/(r + w)$ of the long-range order parameter, where r and w represent the number of *right* atoms (e.g., Ni (Al) atoms on Ni (Al) sites) and *wrong* atoms (e.g., Ni (Al) atoms on Al (Ni) sites or impurity atoms, or even vacancies, on both Ni and Al sites), **S** attains its maximum value $\mathbf{S} = 1$ only for the *completely ordered* compound Ni_3Al when $w = 0$ and is bound to be *less than unity* when $w \neq 0$. The most remarkable feature of the above definition is that it permits a reasonably accurate determination of the site occupation of Ni and Al sublattices. To illustrate this point, we take the example of the 'quenched' sample S_2 for which the observed value of **S** is (table 1) $\mathbf{S}_{obs} = 0.76(4)$. For the Ni (Al) sublattice, $r + w = 75$ (25) and the value $\mathbf{S}_{cal} = 0.76 = (r - w)/(r + w)$ yields $r - w = 57$ (19). It immediately follows that the numbers of right and wrong atoms on the Ni (Al) sublattice are $r = 66$ (22) and $w = 9$ (3), respectively. Note that the *antisite* concentrations are in the *ratio* 3:1, as expected. Alternatively, the above result implies that in this sample, Ni (Al) atoms occupy 88% (12%) of the Ni sites while the Al (Ni) atoms occupy 88% (12%) of Al sites. Thus, the values of **S** displayed in table 1 yield the percentage of Ni (Al) sites occupied by Ni and Al atoms for the samples S_0, S_1, S_2 as 92.0, 97.5, 88.0 (8.0, 2.5, 12.0) and 8.0, 2.5, 12.0 (92.0, 97.5, 88.0), respectively. The above calculation, however, does not allow for the presence of impurity atoms or vacancies on the Ni sublattice or Al sublattice or both Ni and Al sublattices. While a very low impurity content of the samples in question does not significantly alter the above-mentioned site occupation of the Ni and Al sublattices, an *appreciable* change in the number of Ni and Al sites that are either occupied by *wrong* atoms or are *vacant* is expected particularly in the '*quenched*' sample S_2, which should have a *very high* concentration of *vacancies*/defects. The latter inference is consistent with the observation [10] that the sample S_2 is extremely *brittle* compared to the samples S_0 and S_1. To elucidate this point further, for the same observed value of $\mathbf{S}_{obs} = 0.76$, one *vacant* Ni (Al) site corresponds to one Al (Ni)

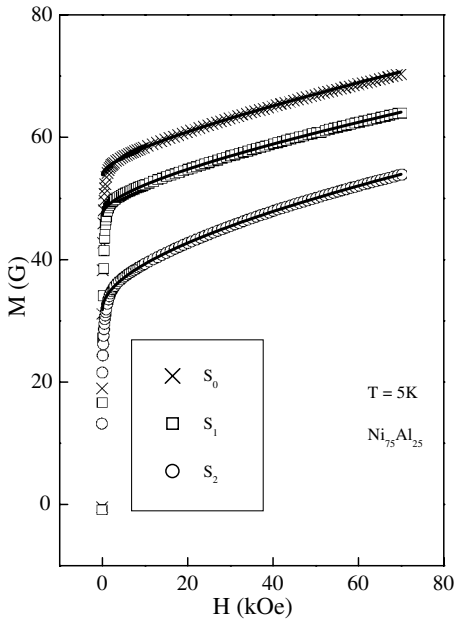

Figure 1. $M(H)$ isotherms at $T = 5$ K. The continuous curves through the data represent the best least-squares fits based on equation (1) of the text.

atom *missing* from the Ni (Al) sublattice and presumably *located* at the *interstitial position.* In other words, point defects can produce a much higher degree of site/bond disorder for the same observed value of **S** and thereby cause sizable changes in the magnetic properties.

The spontaneous magnetization, $M(T, 0)$, or, equivalently, the magnetic moment per Ni atom (μ_{Ni}) and high-field susceptibility (χ_{hf}) at $T = 5$ K, were determined by fitting the expression

$$M(T, H) = M(T, 0) + \eta'\sqrt{H} + \chi_{\mathrm{hf}} H \tag{1}$$

to the $M(T, H)$ isotherm taken at $T = 5$ K for fields above the technical saturation. The technical saturation (the 'knee') in the $M(T = 5\ \mathrm{K}, H)$ curves sets in at $H \approx 1.5$ kOe, 1.5 and 2.5 kOe in the samples S_0, S_1 and S_2, respectively. In equation (1), the $\sqrt{H}$ term accounts for the suppression of spin waves by the field H. The $M(T, H)$ data (symbols) and the best least-squares fits (continuous curves), based on equation (1), are shown in figure 1, while the corresponding values of the fitting parameters μ_{Ni} (deduced from $M(T, 0)$), η' and χ_{hf} are listed in table 1. A cross-check for the values of μ_{Ni} so obtained is provided by the results of the following alternative method. In this approach, $[M(T, H)]^2$ versus $H/M(T, H)$ (Arrott) plots at different temperatures, based on the magnetic equation of state [4, 5]

$$H/M(T, H) = a(T) + b\{(3\langle m_{||}^2\rangle + 2\langle m_{\perp}^2\rangle) + [M(T, H)]^2\}, \tag{2}$$

are constructed out of the raw $M(T, H_{\mathrm{ext}})$ data. Such plots are shown in figure 2 for all three samples (SQUID data at 5 K) and in figure 3 for the samples S_1 and S_2 only (VSM data at $T \geqslant 14.7$ K). The linear high-field portions of the Arrott plot isotherms are extrapolated to $H = 0$, as shown in figures 2 and 3, to yield the intercepts on the ordinate axis equal to the spontaneous magnetization squared, $[M(T, 0)]^2$, at different temperatures. The $M(T, 0)$ data, obtained in this way, together with the 'in-field' magnetization data at a few selected values of H_{ext} in the interval 1 kOe $\leqslant H_{\mathrm{ext}} \leqslant 4$ kOe, are shown in figure 4. For a given sample, the

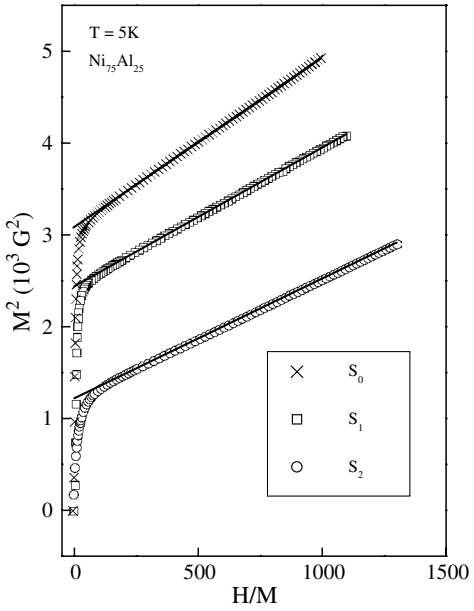

Figure 2. Arrott (M^2 versus H/M) plots constructed out of the $M(H)$ isotherms taken at $T = 5$ K. The solid straight lines represent the theoretical fits to the high-field data based on equation (2) of the text.

Table 2. The Curie temperature, T_C, spin wave stiffness at 0 K, D_0, D_0/T_C ratio and coefficients/prefactors A'', $A'(H = 0)$ and $A(H = 0)$ appearing in equations (5*b*), (7) and (6*c*), respectively.

Sample	T_C (K)	D_0 (meV Å^2)	D_0/T_C (meV Å^2 K^{-1})	A'' (10^{-4} K$^{-4/3}$)	$A'(H=0)$ (10^{-4} K^{-2})	$A(H=0)$ (10^{-3} K$^{-4/3}$)
S_0	56.50(5)	68.2(8)	1.21(2)	—	—	—
S_1	56.38(5)	69.6(4)	1.23(2)	7.27(3)	3.12(2)	4.65(3)
S_2	36.00(5)	45.3(7)	1.26(2)	45.0(2)	25.0(2)	8.23(3)

above two methods yield the same value for μ_{Ni} (deduced from $M(T, 0)$ at $T = 5$ K) within the uncertainty limits. In addition, the Arrott plots yield values (table 2) of the Curie temperature, T_C (i.e., the temperature at which the linear M^2–(H/M) isotherm passes through the origin in figure 3 or, alternatively, the temperature at which $M(T, 0)$ goes to zero in figure 4), that agree quite well with those obtained by the kink-point method [8].

According to the Stoner–Wohlfarth model (SWM), the magnetization for both $H = 0$ and $H \neq 0$ over the entire temperature range $0 \leqslant T \leqslant T_C$ is given by [11, 12]

$$[M(T, H)]_{SWM} = M(0, H)[1 - a(H)T^2] \tag{3}$$

with the Stoner Curie temperature, T_C^S, related to the coefficient of the T^2 term as $a(H = 0) = (T_C^S)^{-2}$. By contrast, the 'conventional' spin fluctuation (CSF) theories [5, 6] and 'modified' spin fluctuation (MSF) model [4] predict different expressions for magnetization in different temperature regions. These expressions are

$$[M(T, 0)]_{MSF} = M(0, 0) - g\mu_B\zeta(3/2)[k_BT/4\pi D(T, 0)]^{3/2}, \qquad H = 0, \tag{4a}$$

$$[M(T, H)]_{MSF} = M(0, H) - g\mu_B Z(3/2, t_H)[k_BT/4\pi D(T, H)]^{3/2}, \qquad H \neq 0, \tag{4b}$$

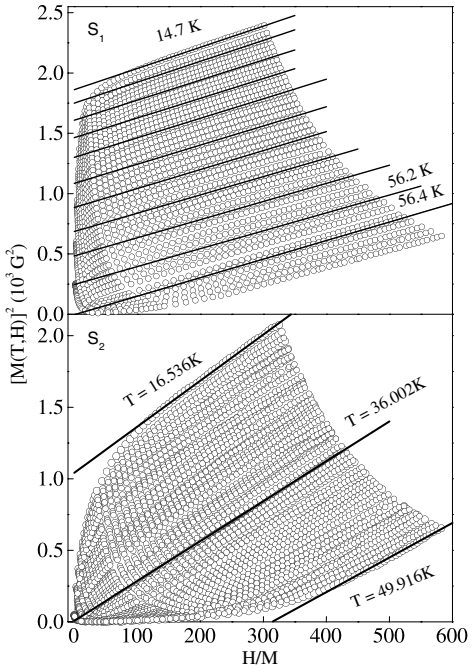

Figure 3. Arrott (M^2 versus H/M) plot isotherms taken over a wide range of temperatures for samples S_1 and S_2.

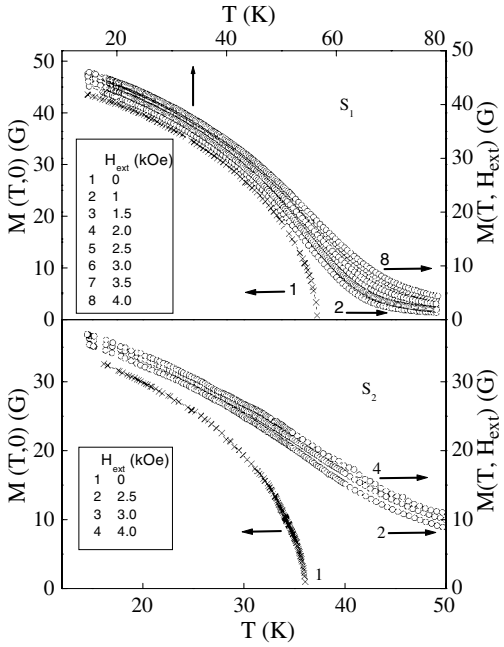

Figure 4. Spontaneous ($H_{ext} = 0$) and 'in-field' ($H_{ext} \neq 0$) magnetization as functions of temperature for the samples S_1 and S_2.

at *low* temperatures,

$$[M(T,0)]_{\mathrm{CSF}} = M(0,0)[1 - a'(0)T^2]^{1/2}, \qquad H = 0, \quad (5a)$$

$$[M(T,H)]_{\mathrm{MSF}} = M(0,H)[1 - A'(H)T^2 - A''T^{4/3}]^{1/2}, \qquad H \neq 0, \quad (5b)$$

at *intermediate* temperatures and

$$[M(T,0)]_{\mathrm{CSF}} = M(0,0)[1 - a''(0)T^{4/3}]^{1/2}, \qquad H = 0, \quad (6a)$$

$$[M(T,H)]_{\mathrm{MSF}} = M(0,H)[1 - A(H)T^{4/3}]^{1/2}, \qquad H \neq 0, \quad (6b)$$

for temperatures *close* to T_{C} ($T \leqslant T_{\mathrm{C}}$) and yet far away from criticality.

In equations (4*a*) and (4*b*), D is the spin wave stiffness and $Z(3/2, t_H)$ is the Bose–Einstein integral function with $t_H = g\mu_{\mathrm{B}}H/k_{\mathrm{B}}T$ which allows for the energy gap in the spin wave spectrum introduced by H_{ext}. Equations (5*b*) and (6*b*) are valid for both $H \neq 0$ and $H = 0$ whereas equations (5*a*) and (6*a*) hold for $H = 0$ only. Moreover, the coefficients of the $T^{4/3}$ terms in equations (6*a*) and (6*b*) for $H = 0$ are completely different [4], i.e., $a''(0) \neq A(H = 0)$, because, unlike the MSF model [4], the CSF theories [5, 6] do not take into account the zero-point spin fluctuations. In sharp contrast with the CSF theories, the MSF model predicts a *specific functional form* for the dependence of the coefficient A of the $T^{4/3}$ term in equation (6*b*) on field H, which is given by [4]

$$A(H) = A(H = 0)[1 - \eta\sqrt{H}]. \quad (6c)$$

3.1. The low-temperature regime

In the absence of spontaneous and 'in-field' (VSM) magnetization data for $T < 14$ K, the 'range-of-fit' analysis [7] of the $M(T, H)$ SQUID data taken at $H_{\mathrm{ext}} = 1$ kOe (that extend down to 5 K) in the low-temperature region has been attempted on the basis of equations (3), (4*b*) and (5*b*). In this analysis, $M(0, H)$ and $a(H)$ in equation (3), $M(0, H)$ and spin wave stiffness D in equation (4*b*), and $M(0, H)$ and $A'(H)$ (note that A'' turns out to be negligibly small in this temperature range and hence is completely dispensed with in this analysis) in equation (5*b*) are treated as free fitting parameters. The final outcome of this exercise is that equation (4*b*) forms *the best* description of the observed temperature dependence of the magnetization in the temperature interval $5\ \mathrm{K} \leqslant T \leqslant 0.25T_{\mathrm{C}}$. The best least-squares (LS) fits (continuous curves in figure 5(a)) to the $M(T, H)$ data (symbols) in this temperature range, based on equation (4*b*), yield the values of D for the samples investigated here listed in table 2. The percentage deviation of the data from the LS fits based on equation (3) (open circles), equation (4*b*) (solid circles) and equation (5*b*) (crosses) in the temperature intervals $0.09T_{\mathrm{C}} \leqslant T \leqslant 0.21T_{\mathrm{C}}$, $0.09T_{\mathrm{C}} \leqslant T \leqslant 0.23T_{\mathrm{C}}$ and $0.14T_{\mathrm{C}} \leqslant T \leqslant 0.28T_{\mathrm{C}}$ for the samples S_0, S_1 and S_2 is plotted against the reduced temperature T/T_{C} in figure 5(b). It is evident from this figure that the *percentage deviation* of the $M(T, H)$ data from the best M–$T^{3/2}$ fit based on equation (4*b*) does not exceed ± 0.005 for S_1 and S_2 (± 0.03 for S_0) and is *evenly* distributed around the theoretically calculated values, whereas the optimum M–T^2 and M^2–T^2 fits, based on equations (3) and (5*b*), respectively, present *systematic* deviations from the data that are as large as $\pm 0.1\%$ for all the samples. The results of the 'range-of-fit' analysis of the $\mathbf{M}(T, H)$ data on S_0, S_1 and S_2, and $\mathbf{M}(T, 0)$ data on S_1, in which $\mathbf{M}(0, 0)$ or $M(0, H)$ and D are varied to optimize agreement between theory and experiment, reveal that for all three samples

(i) equations (4*b*) and (4*a*) provide the best description of the data for $T \leqslant 0.28T_{\mathrm{C}}$ (continuous curves in figure 5(a)),

(ii) for a given sample, spin wave stiffness possesses the *same* value (within the uncertainty limits) regardless of the magnitude of the field in the interval $0 \leqslant H_{\mathrm{ext}} \leqslant 15$ kOe and

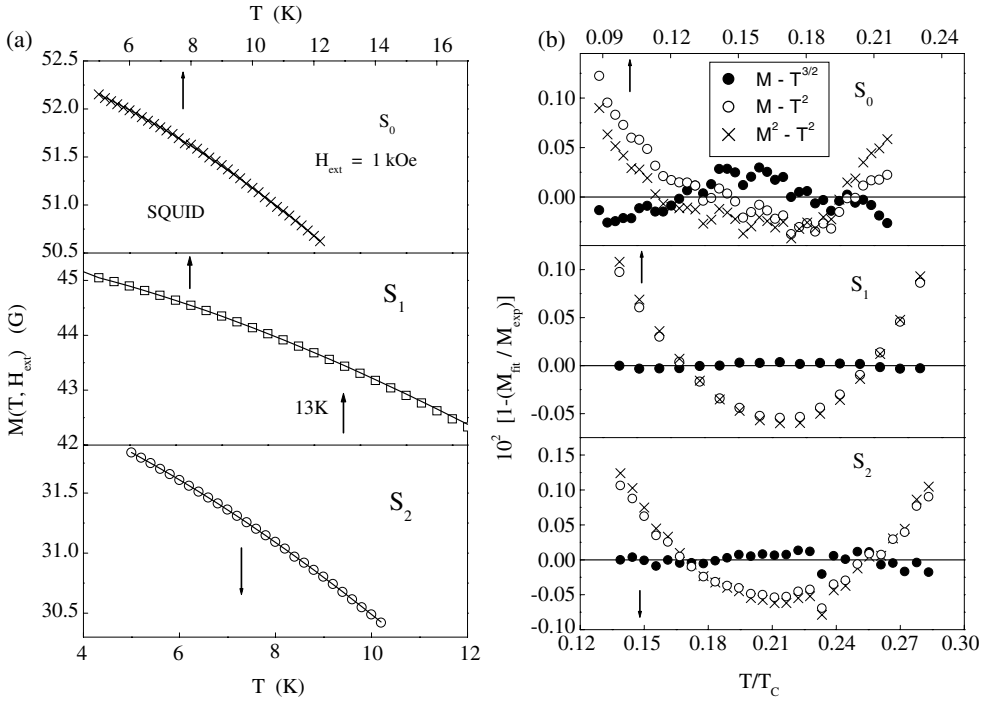

Figure 5. (a) $M(T, H_{\rm ext})$ data at $H_{\rm ext} = 1$ kOe. Continuous curves depict the fits based on equation (4*b*) at low temperatures. (b) Percentage deviation of $M(T, H_{\rm ext} = 1$ kOe) data from the best least-squares fits based on equations (3)–(5) at low temperatures.

(iii) $M(0, H_{\rm ext})$ values yielded by the best LS fits, based on equation (4*b*), conform very well [7] with the $M(T, H_{\rm ext})$ values measured at $T = 5$ K with the SQUID magnetometer.

Moreover, the versions of equation (4) that take into account the temperature renormalization of D, when used for analysis, did not result in any improvement in the quality of the fits. Thus the values of D determined in this work are those of spin wave stiffness at 0 K, D_0.

The final values of D_0 for various samples, considering the variation in the value of D_0 not only for a given data set but also from one set to another as the temperature range of the fit is changed, with a conservative assignment of errors, are displayed in table 2. The value for the annealed sample S_1, i.e., $D_0 = 69.60$ meV Å^2, compares favourably with $D_0 = 70(20)$ meV Å^2 ($D_0 = 85(15)$ meV Å^2) determined in the temperature range 5 K $\leqslant T \leqslant$ 15 K (at $T = 20.4$ K) from the small-angle neutron scattering [13] (inelastic neutron scattering [14]) data. From a detailed comparison between the different types of theoretical fits to the magnetization data (figures 5(a), (b)) and the agreement between the values of the spin wave stiffness determined by different experimental techniques, it is concluded that spin wave excitations *dominantly* contribute to the thermal demagnetization of both spontaneous and 'in-field' magnetizations for temperatures $T \leqslant 0.28T_{\rm C}$. Moreover, from the data presented in tables 1 and 2, it is evident that site disorder *decreases* both the spin wave stiffness, D_0, and the Curie temperature, $T_{\rm C}$, but leaves the value of the $D_0/T_{\rm C}$ ratio essentially unaltered.

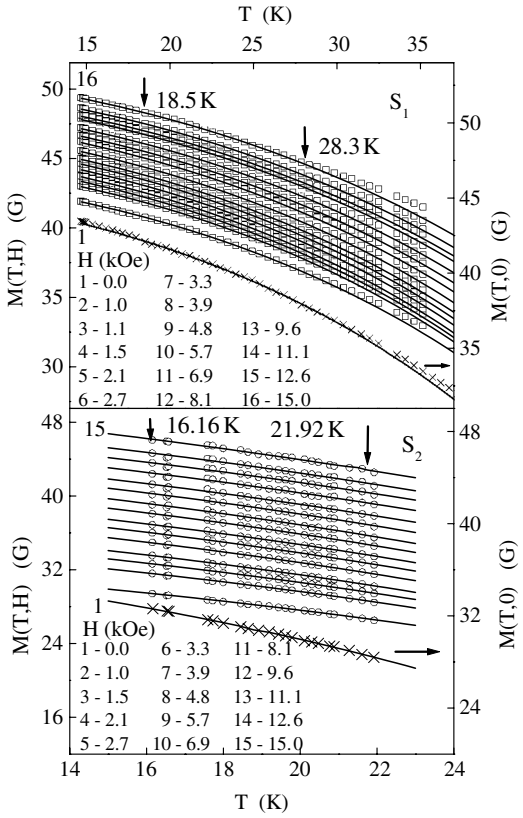

Figure 6. $M(T)$ data at intermediate temperatures for various values of H. Continuous curves depict the fits based on equation (5*a*) for $M(T, 0)$ and equation (5*b*) for $M(T, H)$.

3.2. The intermediate-temperature range

An exhaustive 'range-of-fit' analysis [7] of the $M(T, H)$, $M'(T, H)$ and $M(T, 0)$ data in the intermediate-temperature range based on equations (3)–(5) yields the following important results.

(i) Of all the theoretical expressions considered, equation (5*b*) alone provides the best LS fit (depicted by the continuous curves in figure 6 (VSM data at $H = 0$ and $H \neq 0$) and figure 7(a) (SQUID data at $H_{\text{ext}} = 1$ kOe)) to the magnetization data at all fields including $H = 0$ and at temperatures ranging between $0.32T_{\text{C}}$ and $0.62T_{\text{C}}$ for the samples under consideration, as is evident from the typical percentage deviation plot shown in figure 7(b).

(ii) The lower and upper limits of the temperature range over which equation (5*b*) completely accounts for the observed temperature dependence of the magnetization do not exhibit any systematic variation with H.

(iii) The coefficient A'' is *field independent* and has the values $A'' = 7.27(3) \times 10^{-4}$ K$^{-4/3}$ and $4.50(2) \times 10^{-3}$ K$^{-4/3}$ for S_1 and S_2 for the values of H ranging between 0 and 15 kOe whereas A' varies with H as shown in figure 8.

A *linear* relation between A' and H of the type

$$A'(H) = A'(H = 0)(1 - \alpha H) \tag{7}$$

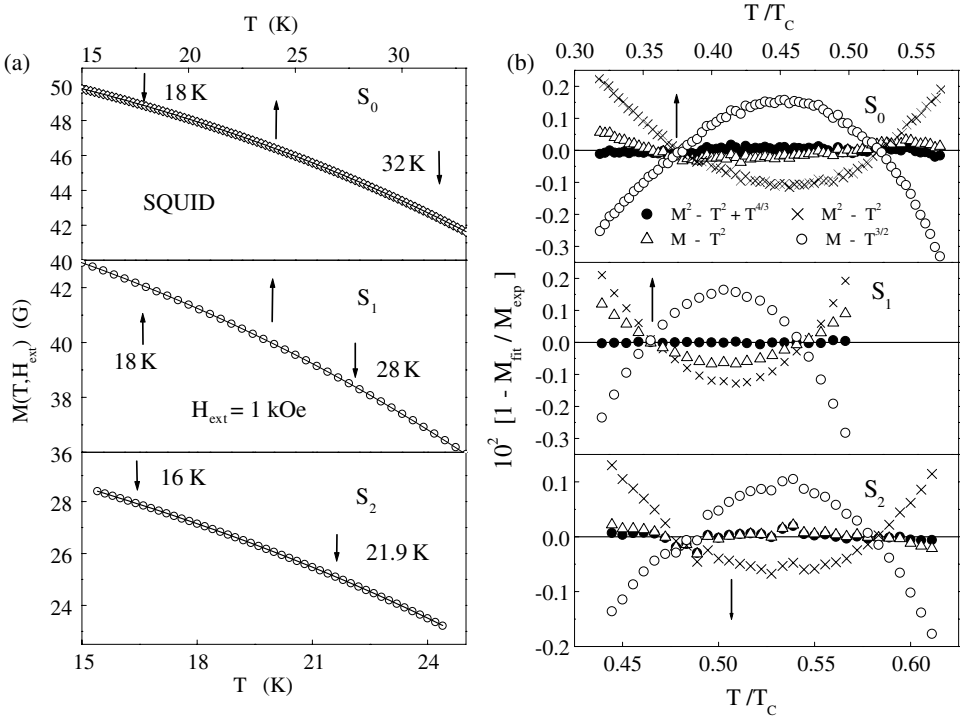

Figure 7. (a) $M(T, H_{\rm ext})$ data at $H_{\rm ext} = 1$ kOe. Continuous curves depict the fits based on equation (5*b*) in the intermediate-temperature region. (b) The percentage deviation of $M(T, H_{\rm ext} = 1$ kOe) data from the best least-squares fits based on equations (3)–(5) at intermediate temperatures.

and an abrupt change in slope, α, at $H^* = 8$ kOe are apparent. The LS fits, based on equation (7), attempted to the $A'(H)$ data and depicted in figure 8 by the straight lines yield the values of the slope as $\alpha = 2.12(13) \times 10^{-5}$ Oe^{-1} ($1.37(2) \times 10^{-5}$ Oe^{-1}) and $1.05(10) \times 10^{-5}$ Oe^{-1} ($7.67(15) \times 10^{-6}$ Oe^{-1}) in the field ranges $0 \leqslant H \leqslant 8$ kOe and 8 kOe $\leqslant H \leqslant 15$ kOe for the sample S_1 (S_2). A linear field dependence of the coefficient of the T^2 term in equation (5*b*) of the form of equation (7) has also been previously observed [15] for fcc Fe–Ni Invar alloys with Ni concentrations in at.% of 34.2, 35.4 and 37.0 in the *intermediate*-temperature range. Like Ni_3Al, these alloys exhibit weak itinerant-electron ferromagnetism. While for the annealed sample S_1 (which has the *highest* degree (95%) of atomic order; table 1) the present value of $A'(H = 0) = 3.12(2) \times 10^{-4}$ K^{-2} (figure 8) compares well with the previously reported [1, 16] value of $A'(H = 0) = 3.92 \times 10^{-4}$ K^{-2} for *ordered* Ni_3Al, the slope α for $H \geqslant 8$ kOe, for the sample S_1, possesses a value that is exactly one order of magnitude *larger* than that ($1.2(2) \times 10^{-6}$ Oe^{-1}) determined earlier [15] for fcc Fe–Ni Invar alloys in the field range 8 kOe $\leqslant H \leqslant 52.7$ kOe.

The above comparison between theory and experiment permits us to draw the following conclusions for the intermediate-temperature range. In conformity with the predictions of the 'modified' spin fluctuation model [4], at intermediate temperatures, the thermally excited spin fluctuations, which manifest themselves as the T^2 term in equation (5*b*), *dominantly* contribute to the thermal demagnetization of $M(T, 0)$ and $M(T, H)$ and get *strongly* suppressed by the magnetic field (equation (7) and figure 8) whereas the zero-point spin fluctuations, which are mainly responsible for the $T^{4/3}$ term in equation (5*b*), make a *small but significant* contribution to the decreases of $M(T, 0)$ and $M(T, H)$ with increasing temperature and are *not affected* by

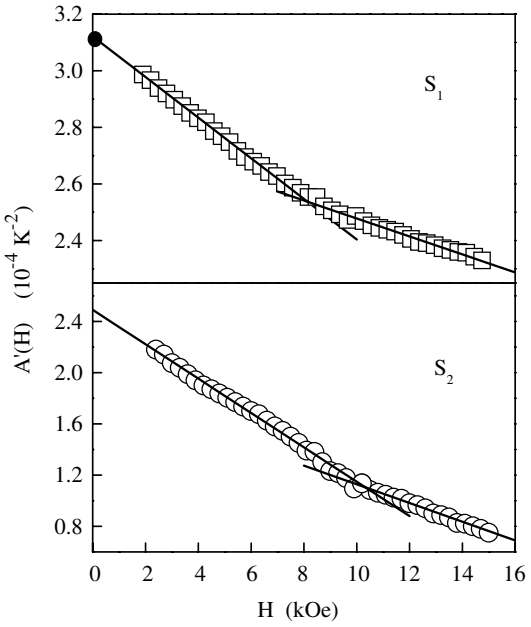

Figure 8. Variation of the coefficient of the T^2 term in the equation (5*b*) with field. The linear fits (solid straight lines) with a slope change at $H \sim 8$ kOe are based on equation (7) of the text.

the field. However, this model, like the 'conventional' spin fluctuation theories [5, 6], does not offer any explanation for the linear field dependence of A' and an abrupt decrease (by roughly a factor of 2) in the value of the slope α at $H^* = 8$ kOe for the samples S_1 and S_2.

3.3. Temperatures below T_C but outside the critical region

For temperatures below T_C but outside the critical region, the following observations have been made on the basis of the 'range-of-fit' analysis of the magnetization data in terms of equations (3), (5) and (6). (a) Irrespective of the degree of site disorder, the observed temperature variation of the spontaneous magnetization ('in-field' magnetization) at such temperatures is best described by equation (6*a*) or equivalently by equation (6*b*) with $H = 0$ (equation (6*b*)), as is clearly apparent not only from the fits (straight lines) to the data (symbols) in figure 9(a) and the percentage deviation plot (which is *representative* of similar plots at other values of H, including $H = 0$, as well) displayed in figure 9(b) but also from the data presented in figure 10. The temperature range over which $[M(T, H)]^2$ varies with temperature as $T^{4/3}$ *broadens* while the slope $A(H)$ of the $[M(T, H)]^2$ versus $T^{4/3}$ straight lines (equation (6*b*)) *decreases* as H *increases*. Figure 11 demonstrates that, in accordance with the prediction (equation (6*c*)) of the MSF model [4], $A(H)$, the coefficient of the $T^{4/3}$ term in equation (6*b*) varies with H as $\sqrt{H}$. Moreover, the best least-squares fits to the $A(\sqrt{H})$ data, based on equation (6*c*), represented by the continuous straight lines in figure 11, yield exactly the same value of $A(H = 0)$ upon extrapolation to $H = 0$ as is obtained directly from the $[M(T, 0)]^2$ versus $T^{4/3}$ plot (figure 10). The observation that the relation $A(H) \sim \sqrt{H}$, i.e., equation (6*c*), holds for fields in the range $0 \leqslant H \leqslant 15$ kOe in the case of *amorphous* weak itinerant-electron ferromagnets as well has been made previously [17]. Thus, the expression for $A(H)$ predicted by the MSF model [4], equation (6*c*), *quantifies* the suppression of thermally excited spin fluctuations (since they are solely responsible for the $\sqrt{H}$ term) at

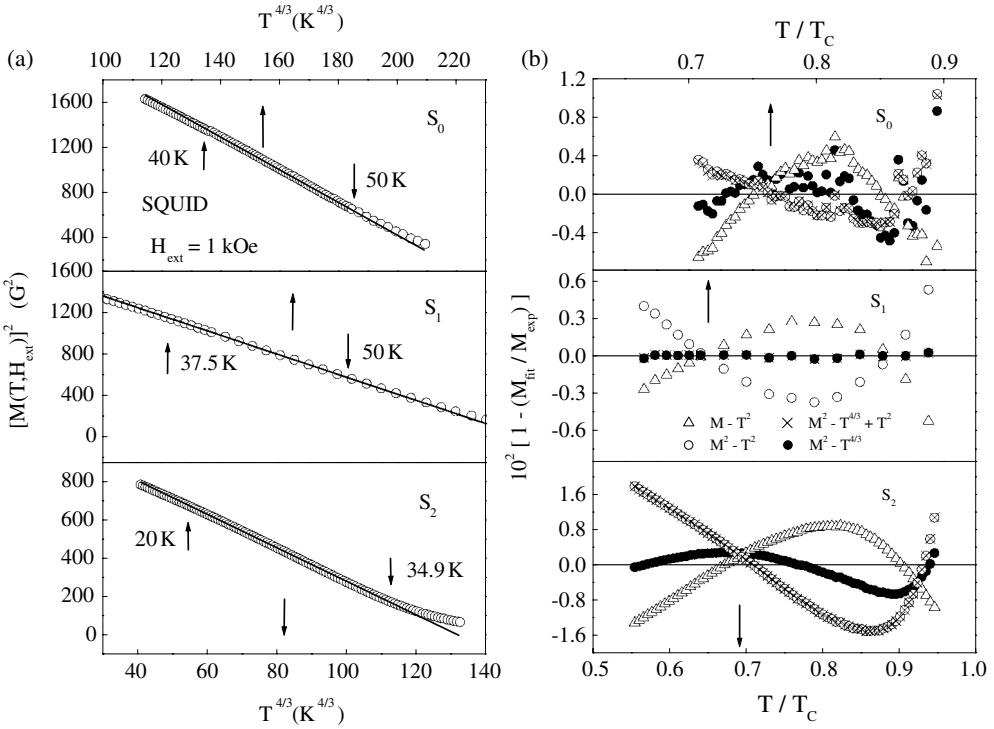

Figure 9. (a) $M(T, H_{\rm ext})$ data at $H_{\rm ext} = 1$ kOe. Continuous curves depict the fits based on equation (6*b*) for temperatures outside the critical region but close to $T_{\rm C}$. (b) The percentage deviation of $M(T, H_{\rm ext} = 1$ kOe) data from the best least-squares fits based on equations (3), (5) and (6) at temperatures close to $T_{\rm C}$.

weak and intermediate fields in weak itinerant-electron ferromagnets regardless of whether they are crystalline (with or without quenched random-exchange disorder) or amorphous (with topological as well as quenched random-exchange disorder). Unlike the expression for $A(H)$ obtained by the CSF theories [6] using the electron gas model, equation (6*c*) involves only a *single* fitting parameter η because the value of $A(H = 0)$ can be obtained directly from the spontaneous magnetization data. The values determined here (table 2) for $A(H = 0)$ for the 'annealed' and 'quenched' $Ni_{75}Al_{25}$ samples S_1 and S_2 yield the values for the Curie temperature as $T_{\rm C}^{\rm SF} = 56.2(3)$ and 36.5(5) K when the relation [4] $T_{\rm C}^{\rm SF} = [A(H = 0)]^{-3/4}$ is used. These values of the Curie temperature agree quite well with $T_{\rm C} = 56.45(5)$ and 36.00(5) K, respectively, deduced from the Arrott plot (figure 2). This finding implies that, barring the low-temperature region (where spin waves basically govern the thermal demagnetization of $M(T, 0)$), the temperature dependence of the spontaneous magnetization for $T \leqslant T_{\rm C}$ is primarily determined by the exchange-enhanced spin-density fluctuations.

The following observations bear out clearly that the Stoner single-particle excitations have a negligible role to play in the reduction of $M(T, 0)$ with temperature in Ni_3Al. Rigorous calculations [4], based on the 'modified' spin fluctuation model, reveal that *in addition to* the $T^{4/3}$ term in equation (6*b*), which originates mainly from the thermally excited spin fluctuations (SF), Stoner single-particle (SP) excitations (which are present in the entire temperature range $T \leqslant T_{\rm C}$) give rise to a T^2 term. Thus, the modified version of equation (6*b*), that includes the T^2 term as well, has the *same* form as equation (5*b*) but the origins of the T^2 term in the

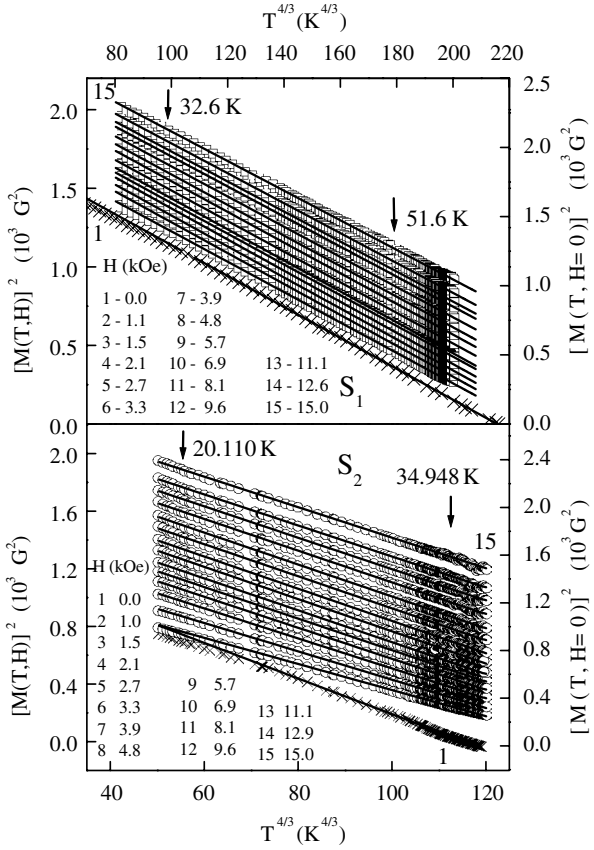

Figure 10. $M(T)$ data at temperatures close to T_C for various values of H. Continuous curves depict the fits based on equation (6*a*) for $M(T, 0)$ and equation (6*b*) for $M(T, H)$.

two equations are different in that the Stoner SP excitations alone (Stoner SP excitations plus SF) contribute to this term in equation (6*b*) (equation (5*b*)). In view of this genesis of the T^2 and $T^{4/3}$ terms, the experimental observation that the percentage deviation has the *same* value (figure 9(b)) for the fits that either include (equation (5*b*)) or exclude (equation (6*b*)) the T^2 term implies that the overwhelmingly large spin fluctuation contribution completely swamps the feeble contribution to $M(T, 0)$ and $M(T, H)$ arising from Stoner SP excitations. The relative importance of spin fluctuations and Stoner SP excitations could not be ascertained at intermediate temperatures because both kinds of excitations make a contribution to $M(T, 0)$ and $M(T, H)$ that varies with temperature as T^2 in this temperature regime. That Stoner SP excitations decrease the magnetization with increasing temperature at a rate which is extremely slow compared to that due to the spin fluctuations has also been previously inferred [18, 19] from the band structure calculations and the results of de Haas–van Alphen effect measurements on Ni_3Al.

3.4. The effect of site disorder

In order to find out the effect of site disorder on the magnetic properties of $Ni_{75}Al_{25}$, the spontaneous magnetization at 0 K, $M(0, 0)$, spin wave stiffness at 0 K, D_0, and Curie

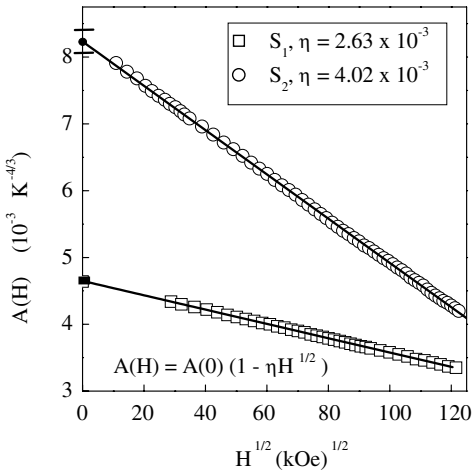

Figure 11. Variation of the coefficient A of the $T^{4/3}$ term in equation (6*b*) with $\sqrt{H}$ for the samples S_1 and S_2. The straight lines through the $A(\sqrt{H})$ data represent the fits based on equation (6*c*) of the text.

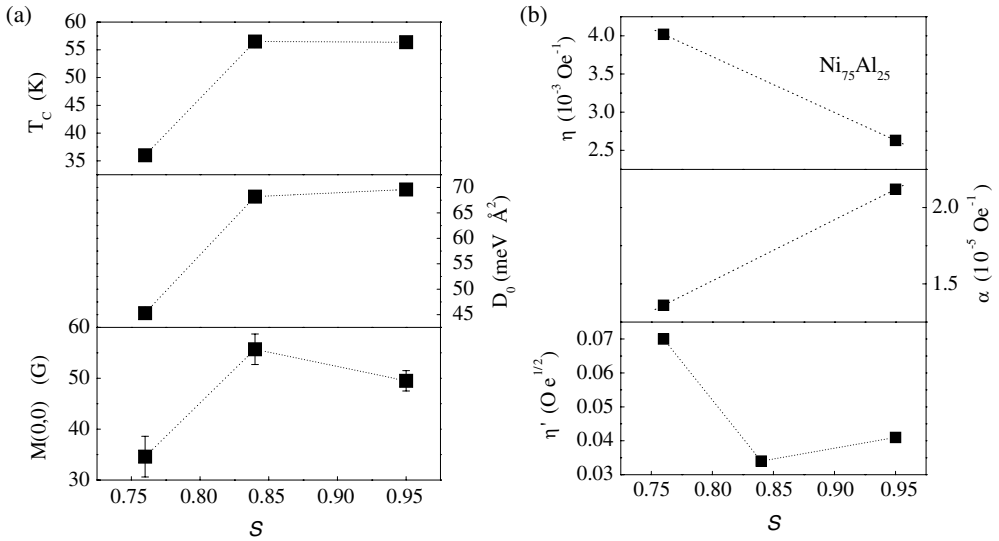

Figure 12. (a) The spontaneous magnetization $M(0, 0)$ at $T = 5$ K, the spin wave stiffness D_0 and the Curie temperature T_C plotted against the atomic long-range order parameter **S**. (b) Variations of the quantities η', α and η, appearing in equations (1), (7) and (6*c*), respectively, with the atomic long-range order parameter **S**.

temperature, T_C, as well as the quantities η', α and η which appear in equations (1), (7) and (6*c*), respectively, are plotted against the atomic long-range order parameter **S** in figures 12(a) and (b). Note that **S** is a direct measure of the site disorder present in the sample in that the *smaller* the value of **S**, the *greater* the degree of site disorder and, for a given value of **S**, the *greater* the concentration of point defects such as vacancies, the *greater* the degree of site disorder. Considering that the coefficient of the $T^{4/3}$ term in the expression (equations (6*b*) and (6*c*)) for the spontaneous magnetization $M(T, 0)$, $A(H = 0)$, is $\sim[M(0, 0)]^{-2}$ [4], its

variation with **S** (table 2) is *consistent* with that of $M(0, 0)$ depicted in figure 12(a). Now that the parameter $\eta'(\eta)$ is not only *inversely proportional* [4] to the spin wave stiffness (the 'stiffness' of local spin-density fluctuations) but also *quantifies* the suppression of spin waves (SW) at low temperatures (thermally excited local spin-density fluctuations (SF) at temperatures close to T_C) with the external magnetic field, the variations of η' and η with **S** shown in figure 12(b) imply that the site disorder *promotes* these low-lying magnetic excitations and makes them *increasingly* sensitive to (or alternatively, SW and SF get *suppressed faster* with) the external magnetic field. Consequently, site disorder reduces both the spin wave stiffness and the Curie temperature. In view of the theoretical prediction [4] that the zero-point (thermally excited) spin fluctuations dominantly (solely) contribute [4] to the $T^{4/3}$ (T^2) term in equation (5*b*) in the intermediate-temperature range (the $T^{4/3}$ power law in the intermediate-temperature range thus happens to be the sole experimental signature of the zero-point fluctuations), the *increased* value (table 2) of the *field-independent* (zero-field) coefficient A'' ($A'(H = 0)$) of the $T^{4/3}$ (T^2) term for the 'quenched' sample S_2 basically reflects the *site disorder-induced enhancement* in the zero-point (thermally excited) spin fluctuations. In sharp contrast with the effect of site disorder on SW and SF excitations at low temperatures and at temperatures close to T_C, site disorder makes the thermally excited spin fluctuations *less sensitive* to the external magnetic field in the intermediate-temperature range, as inferred from the variation of α with **S** displayed in figure 12(b). Moreover, since the zero-point spin fluctuations contribute to $M(T, 0)$ and $M(T, H)$ over the entire temperature range from $T = 0$ K to temperatures well above T_C, the enhancement in zero-point spin fluctuations caused by site disorder also accounts for the decrease in $M(0, 0)$ with decreasing **S** (figure 12(b)). Other important observations that merit attention are as follows.

(i) The quantities of interest, shown in figures 12(a) and (b) and table 2, exhibit a sizable change in their magnitudes when point defects such as vacancies play an important role in enhancing the degree of site disorder (for details, refer to the discussion in the opening paragraph of section 3).

(ii) Site disorder *only affects the magnitude of the suppression* of spin waves and thermally excited spin fluctuations by magnetic field (i.e., the value of η' in equation (1) or the values of $A'(H = 0)$ and α in equations (5*b*) and (7) and those of $A(H = 0)$ and η in equations (6*b*) and (6*c*)), *and not the functional form of the suppression with field* which is $\sqrt{H}$ for spin waves at low temperatures (equation (1)) and *slows down* from a *linear* variation ($A'(H) \sim H$ in equation (7)) at *intermediate* temperatures to a *square root* variation ($A(H) \sim \sqrt{H}$ in equation (6*c*)) at temperatures *close to* T_C for the thermally excited spin fluctuations.

With a view to gaining a deeper physical insight into the role of site disorder, the results are discussed in terms of the following expressions [4, 5] that relate different magnetic parameters of interest:

$$\chi(0, 0) = N\mu_B^2 N(E_F)\mathcal{S}, \tag{8}$$

$$[M(0, 0)]^2 = (N\mu_B\mu_0)^2 = (\mathcal{S}\gamma)^{-1}, \tag{9}$$

$$\mathcal{S} = [IN(E_F) - 1]^{-1}, \tag{10}$$

$$\gamma = (1/2)\{N\mu_B N(E_F)\}^{-2}\{N'(E_F)/N(E_F)]^2 - [N''(E_F)/3N(F_F)]\}, \tag{11}$$

$$D_0 = g\mu_B c_\perp M(0, 0) \tag{12}$$

$$T_C = \left(\frac{2\pi^2}{5\alpha}\right)^{3/4} [M(0, 0)]^{3/2}(\hbar\gamma_v)^{1/4}\left(\frac{c_v}{k_B}\right), \tag{13}$$

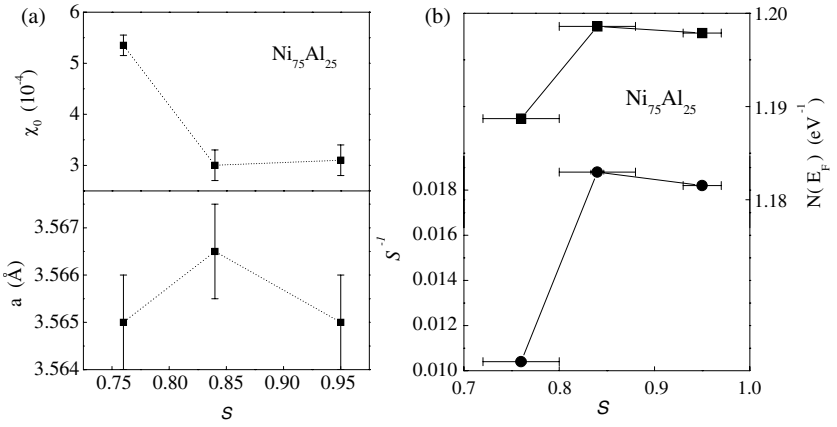

Figure 13. (a) Variations of the lattice parameter a and zero-field differential susceptibility χ_0 with the atomic long-range order parameter **S**. (b) Variations of the inverse Stoner enhancement factor $\mathcal{S}^{-1}$ and density of states at the Fermi level $N(E_F)$ with the long-range atomic order parameter **S**. Note that the error bars in $N(E_F)$ and $\mathcal{S}^{-1}$ are smaller than the size of the data symbols.

where $\chi_0 \equiv \chi(0,0)$, μ_0 and $M_0 \equiv M(0,0)$ are the zero-field differential susceptibility, moment per alloy atom and spontaneous magnetization at 0 K, respectively, I and $\mathcal{S}$ are the Stoner parameter and Stoner enhancement factor, $N'(E_F)$ and $N''(E_F)$ are the first and second energy derivatives of the density of states at the Fermi level, $N(E_F)$, respectively. N is the number of atoms per unit volume. The expressions for the quantities c_v and γ_v involve the energy derivatives [5] of $N(E_F)$ and hence, like γ, depend on the shape of the density of states (DOS) curve near the Fermi level, E_F.

The variations of the lattice parameter a and χ_0 (determined from the slope $b^{-1} = 2\chi_0 M_0^2$ and the intercept on the ordinate $M_0^2 = -a(T = 5\text{ K})/b$ of the Arrott plot at $T = 5$ K, based on equation (2) and shown in figure 2) with the atomic long-range order parameter **S** are depicted in figure 13(a), while the values of the density of states at the Fermi level, $N(E_F)$, and the inverse Stoner enhancement factor $\mathcal{S}^{-1}$, computed using the observed values of χ_0 and the previously reported [20] value of the Stoner parameter $I = 0.85$ eV in equations (8) and (10), are plotted against **S** in figure 13(b). It is evident from the data presented in figure 13 that site disorder has *practically no influence* on the lattice parameter but *reduces* $N(E_F)$ and hence $\mathcal{S}^{-1}$. To ascertain whether or not the reduction in $N(E_F)$ is associated with the smearing out of the sharp features of the DOS curve near E_F, we proceed as follows. Equations (9) and (11) are recast into an alternative form, i.e.,

$$M_0 = N\mu_B(2\beta)^{1/2}[N(E_F)]^2(\mathcal{S}^{-1})^{1/2} \tag{14}$$

with

$$\beta = \{[N'(E_F)]^2 - [N''(E_F)N(E_F)/3]\}^{-1}, \tag{15}$$

so that the dependences of M_0 on $N(E_F)$ and the shape of the DOS curve near E_F (reflected in the band parameter β) are brought out explicitly. If site disorder affects only $N(E_F)$ and not β, M_0 should vary *linearly* with $[N(E_F)]^2(\mathcal{S}^{-1})^{1/2}$. The *nonlinear* M_0 versus $[N(E_F)]^2(\mathcal{S}^{-1})^{1/2}$ plot, shown in figure 14, implies that the site disorder does change the shape of the DOS curve near E_F, besides reducing $N(E_F)$. The sharp features in the DOS curve near E_F are presumably smeared out by the distribution in the nearest-neighbour Ni–Ni distances caused by site disorder.

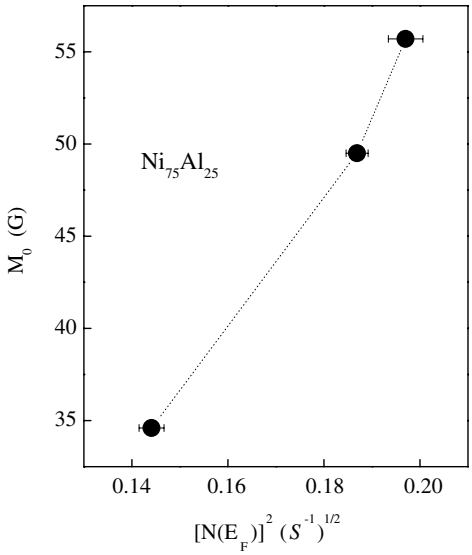

Figure 14. The spontaneous magnetization M_0 plotted against the quantity $[N(E_F)]^2(\mathcal{S}^{-1})^{1/2}$ (see the text).

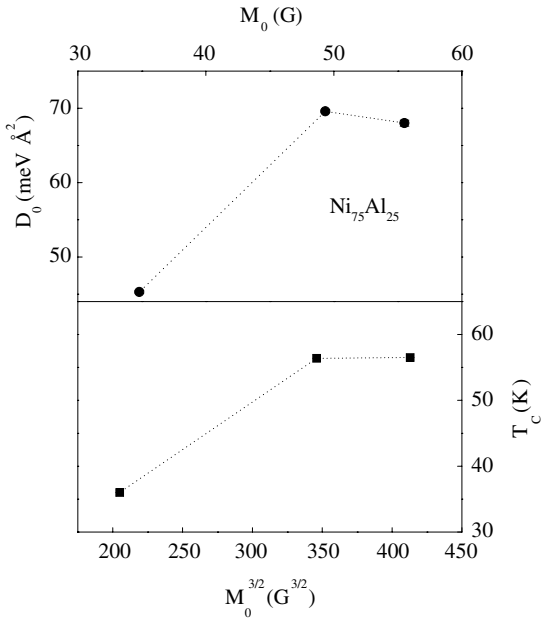

Figure 15. The D_0 versus M_0 and T_C versus $M_0^{3/2}$ plots.

Similarly, in the case where the band parameters $c_\perp$, c_v and γ_v (which are *sensitive* to the shape of the DOS curve near E_F) do not vary with site disorder, equations (12) and (13) predict that

$$D_0 \sim M_0 \tag{16}$$

and

$$T_C \sim M_0^{3/2}. \tag{17}$$

The plots D_0 versus M_0 and T_C versus $M_0^{3/2}$, displayed in figure 15, re-emphasize the above inference that the site disorder alters the shape of the DOS curve near E_F and reduces $N(E_F)$ (directly reflected in M_0; figure 14).

4. Conclusion

An elaborate analysis of high-resolution magnetization data taken for polycrystalline $Ni_{75}Al_{25}$ samples with varying degree of site disorder permits us to draw the following conclusions regarding the role of site disorder.

(i) Regardless of the degree of site disorder present, spin waves, zero-point plus thermally excited local spin-density fluctuations and non-propagating thermally excited spin fluctuations completely account for the thermal demagnetization of spontaneous and 'in-field' magnetizations in the temperature ranges $0.09T_C \leqslant T \leqslant 0.28T_C$, $0.32T_C \leqslant T \leqslant 0.62T_C$ and $0.65T_C \leqslant T \leqslant 0.95T_C$, respectively.

(ii) Site disorder smears out the sharp features in the density of states (DOS) curve near the Fermi level, E_F, and reduces the DOS at E_F, $N(E_F)$, the spontaneous magnetization at 0 K, M_0, the spin wave stiffness at 0 K, D_0, and the Curie temperature, T_C, but leaves the D_0/T_C ratio essentially unaltered.

(iii) Site disorder only affects the magnitude of suppression of the low-lying magnetic excitations by magnetic field (H) and does not change the functional form of the suppression with H. Alternatively, irrespective of the extent of the site disorder present, the functional form of the suppression with field is $\sqrt{H}$ for spin waves at low temperatures and *slows down* from a *linear* ($\sim H$) variation at intermediate temperatures to a *square root* ($\sim\sqrt{H}$) variation at temperatures close to T_C for the thermally excited local spin-density fluctuations.

Acknowledgment

This work was supported by the Department of Science and Technology, India, under the grant DO No SP/S2/M-21/97.

References

[1] de Boer F R, Schinkel C J, Biesterbos J and Proost S 1969 *J. Appl. Phys.* **40** 1049
[2] Robbins C G and Claus H 1971 *Magnetism and Magnetic Materials* (*AIP Proc.* No. 5) ed C D Graham and J J Rhyne (New York: American Institute of Physics) p 527
[3] Kaul S N, Semwal A and Schaefer H-E 2000 *Phys. Rev.* B **62** 13892
[4] Kaul S N 1999 *J. Phys.: Condens. Matter* **11** 7597
[5] Lonzarich G G and Taillefer L 1985 *J. Phys. C: Solid State Phys.* **18** 4339
[6] Sasakura H, Suzuki K and Masuda Y 1984 *J. Phys. Soc. Japan* **53** 352
Sasakura H, Suzuki K and Masuda Y 1984 *J. Phys. Soc. Japan* **53** 754
Moriya T 1985 *Spin fluctuations in Itinerant Electron Magnetism* (*Springer Series in Solid State Sciences* vol 56) (Berlin: Springer) and references cited therein
[7] Semwal A and Kaul S N 1999 *Phys. Rev.* B **60** 12799
[8] Semwal A and Kaul S N 2002 *J. Phys.: Condens. Matter* **14** 5829
[9] Nelson J B and Riley D P 1945 *Proc. Phys. Soc.* **57** 160
Taylor A and Sinclair H 1945 *Proc. Phys. Soc.* **57** 126

[10] D'Santhoshini B A and Kaul S N 2003 *J. Phys.: Condens. Matter* **15** 4903
[11] Stoner E C 1939 *Proc. R. Soc.* **139** 339
[12] Edwards D M and Wohlfarth E 1968 *Proc. R. Soc.* A **303** 127
[13] Bernhoeft N R, Cole I, Lonzarich G G and Squires G 1982 *J. Appl. Phys.* **53** 8204
[14] Bernhoeft N R, Lonzarich G G, Mitchell P W and Paul D McK 1983 *Phys. Rev.* **28** 422
[15] Nakai I and Maruyana H 1992 *J. Magn. Magn. Mater.* **104–107** 2053
Nakai I 1990 *J. Phys. Soc. Japan* **59** 2211
[16] Chatel P F and de Boer F R 1970 *Physica* **48** 331
[17] Kaul S N and Babu P D 1998 *J. Phys.: Condens. Matter* **10** 1563
Babu P D and Kaul S N 1997 *J. Phys.: Condens. Matter* **9** 3625
[18] Lonzarich G G 1984 *J. Magn. Magn. Mater.* **45** 43
[19] Lonzarich G G 1986 *J. Magn. Magn. Mater.* **54–57** 612
[20] Buis N, Franse J J M and Broumer P E 1981 *Physica* B **106** 1